Optics Communications 284 (2011) 3939–3945

Contents lists available at ScienceDirect

Optics Communications

journal homepage: www.elsevier.com/locate/optcom

Exploiting the speckle noise for compressive imaging

Agnès Delahaies [a], David Rousseau [a,*], Denis Gindre [b], François Chapeau-Blondeau [a]

[a] Laboratoire d'Ingénierie des Systèmes Automatisés (LISA), Université d'Angers, 62 avenue Notre Dame du Lac, 49000 ANGERS, France
[b] Moltech Anjou, UMR CNRS 6200, Université d'Angers, 2 boulevard Lavoisier, 49000 ANGERS, France

ARTICLE INFO

Article history:
Received 28 December 2010
Received in revised form 4 March 2011
Accepted 15 April 2011
Available online 1 May 2011

Keywords:
Compressive imaging
Speckle noise
Coherent imaging
Optical image processing

ABSTRACT

An optical setup is proposed for the implementation of compressive sensing with coherent images. This setup specifically exploits the natural multiplicative action of speckle noise occurring with coherent light, in order to optically realize the essential step in compressive sensing which is the multiplication with known random patterns of the image to be acquired. In the test of the implementation, we specifically examine the impact of several departures, that exist in practice, from the ideal conditions of a pure multiplicative action of the speckle. In such practical realistic conditions, we assess the feasibility, performance and robustness of the optical scheme of compressive sensing.

1. Introduction

Compressive sensing is a recent methodology [1–3] aiming at improving the efficacy of acquisition for many natural information-carrying signals. To exploit its innovative principle, practical implementation of compressive sensing calls for a new generation of acquisition devices and remains an important challenge. When dedicated to images, practical implementations of compressive sensing that have appeared in the domain of optics mainly involved standard incoherent intensity images, often associated with specialized electronic hardware [4–12]. Here, we propose and investigate another candidate approach for a physical implementation of compressive-sensing imaging. We present an optical setup using coherent light supporting a novel technique for implementing compressive imaging. Especially, with coherent light, one can exploit the natural multiplicative action of speckle noise [13,14] in order to realize the essential step in compressive sensing which is the multiplication with known random patterns of the image to be acquired. Such a proposal has recently [15] been made for ghost imaging [16,17]. In [15], the speckle pattern produced by spatial light modulator optoelectronic device are not measured but computed using the Fresnel–Huygens propagator. In this paper, we propose, on the basis of modeling and experimentation, to further analyze the use of the natural multiplicative action of speckle noise to compressive sensing. The speckle pattern here will be produced by a simple diffuser to implement a minimal optical scheme for compressive sensing with coherent light. We expect for compressive sensing a constructive implication of the speckle noise, as it was obtained for another imaging operation in Refs. [18,19]. We specifically study the robustness of the compressive sensing when some departure from a perfect multiplicative action of the speckle is present.

2. The compressive sensing scheme

In compressive sensing [1–3], a signal $\mathbf{x}$ with N scalar components $[x_1, \ldots x_N]^\top = \mathbf{x}$ in some original orthonormal basis of $\mathbb{R}^N$, is considered K-sparse with components $[s_1, \ldots s_N]^\top = \mathbf{s}$ in a transformed orthonormal basis of $\mathbb{R}^N$ where only K components are non-negligible. The change of coordinates $\mathbf{x} = \Psi\mathbf{s} \Leftrightarrow \mathbf{s} = \Psi^{-1}\mathbf{x}$ is expressed through the $N \times N$ unitary matrix Ψ. It is in general not possible to directly measure the K components in the sparsity basis, because their number and locations among N are usually not known, and are also signal-dependent. As a more universal approach, compressive sensing chooses, from the original basis, to measure M (with $K<M<N$) fixed independent linear combinations of the vector $\mathbf{x}$, under the form $\mathbf{y} = [y_1, \ldots y_M]^\top = \Phi\mathbf{x}$ with Φ an $M \times N$ measurement matrix, which is also $\mathbf{y} = \Phi\Psi\mathbf{s} = \mathbf{A}\mathbf{s}$ with $\mathbf{A} = \Phi\Psi$ an $M \times N$ reconstruction matrix. A specific input $\mathbf{x} = \mathbf{x}^0$, with sparse representation $\mathbf{s}^0 = \Psi^{-1}\mathbf{x}^0$, is associated with the measurement vector $\mathbf{y}^0 = \Phi\mathbf{x}^0$. The K-sparse vector $\mathbf{s}^0$ is thus the solution to the underdetermined system $\mathbf{A}\mathbf{s} = \mathbf{y}^0$. Compressive sensing proposes to recover $\mathbf{s}^0$ by seeking the sparsest solution to this system. This is usually done through solving

$$\hat{\mathbf{s}} = \arg\min_{\mathbf{s}} \|\mathbf{A}\mathbf{s} - \mathbf{y}^0\|_2 + \lambda\|\mathbf{s}\|_1, \tag{1}$$

with $\lambda > 0$ a regularization parameter, which is a convex optimization problem that can be solved efficiently by linear programming techniques. The non-observed input $\mathbf{x}$ then follows as $\hat{\mathbf{x}} = \Psi\hat{\mathbf{s}}$. The effectiveness of this scheme has been shown, for many natural signals, when the

* Corresponding author.
E-mail address: david.rousseau@univ-angers.fr (D. Rousseau).

0030-4018/$ – see front matter © 2011 Elsevier B.V. All rights reserved.
doi:10.1016/j.optcom.2011.04.036

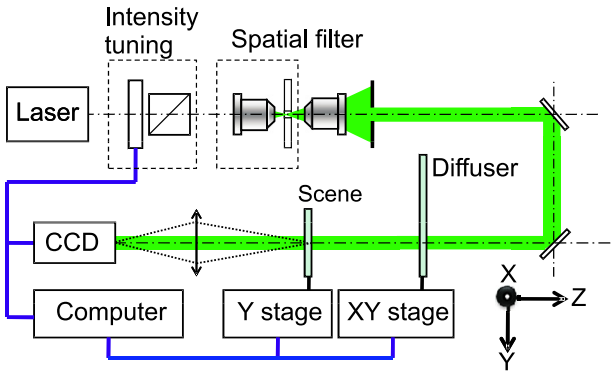

Fig. 1. Experimental setup for an optical implementation of compressive sensing with coherent light. The intensity tuning block together with the spatial filter are used to obtain an almost uniform beam with no saturation of the CCD camera. The laser light traversing a static diffuser taken as a frosted glass produces the speckled beam, which then illuminates the imaged scene, a slide with calibrated transparency levels carrying the contrast of the input image to be compressed. The lens images the scene plane on the CCD matrix of the camera.

measurement matrix Φ is an $M\times N$ random matrix, realized by assembling M random vectors $\boldsymbol{\phi}^m=[\phi_1^m, \ldots \phi_N^m]^\top$ with independent components for $m=1$ to M, to yield $\Phi=[\boldsymbol{\phi}^1|\boldsymbol{\phi}^2| \ldots |\boldsymbol{\phi}^M]^\top$. Each measurement y_m is thus constructed as the inner product

$$y_m = (\boldsymbol{\phi}^m)^\top \mathbf{x} = \sum_{n=1}^{N} \phi_n^m x_n, \tag{2}$$

interpretable as the random projections of the input vector $\mathbf{x}$ on M random vectors $\boldsymbol{\phi}^m$.

For compressive imaging, we treat an image by vectorizing it into a long $N\times 1$ column vector. It has recently been proposed to consider images in 2-D matrices for compressive sensing to preserve the natural spatial sparsity of images [20]. In this study, we choose to work with images coded in a column vector as the original simplest transposition of compressive sensing to images. An explicit transformed basis has to be chosen in which the input vector $\mathbf{x}$ is supposed to be sparse. In this study, we choose to work with binary images. An appropriate choice of basis (although others may also do) for binary images is a Walsh basis, when $\boldsymbol{\Psi}$ is a Hadamard matrix implementing a Hadamard transform [21]. The input binary image $\mathbf{x}$ is thus assumed sparse in this Walsh-Hadamard basis. From the measurement vector $\mathbf{y}$, reconstruction is then performed by numerically solving the convex optimization problem of Eq. (1) with the method of [22].

3. An optical compressive imaging setup

An essential step in the compressive sensing scheme reviewed in Section 2 is the random projections of Eq. (2). We describe the experimental implementation of this essential step of the compressive sensing by exploiting speckle noise. When a beam of light traverses a transparent medium, the light intensity across the transmitted beam is the product of the incident beam profile by the spatial transparency of the medium [13,14]. An all-optical product is realized in this way, with incoherent as well as with coherent light. In addition, with coherent light, when the medium traversed by a coherent beam incorporates strong spatial irregularities at the wavelength scale, a speckle pattern is formed across the transmitted wavefront and acts multiplicatively on the incident coherent beam. The speckle pattern exhibits a noise-like grainy appearance but at the same time it is deterministically determined by the microscale irregularities imprinted in the transparent medium. In this way, by exploiting a speckled beam, there is, in principle, the possibility of obtaining the controllable random patterns that will act multiplicatively to realize the random projections of Eq. (2) constructing the measurements in compressive sensing.

To test this proposal in practice, we build the optical setup presented in Fig. 1. In this optical setup, a laser beam is passed through a static diffuser with strong spatial irregularities at the wavelength scale, in order to produce a speckled beam carrying a random pattern with strong spatial irregularities. Different patterns of random speckle are obtained by translating the static diffuser with an XY micro-sensitivity stage at a step larger than the beam diameter. The input image to be compressed, denoted as the scene in Fig. 1, is printed on a transparent slide to perform a product when it receives the speckled beam. Each speckle pattern $\Phi(u, v)$ where (u, v) are the spatial coordinates, produced at the output of the diffuser is first measured separately, in the absence of the scene to be imaged. Then, for each position of the diffuser, the scene $X(u, v)$ is introduced in the speckled beam to experience the multiplication by the known random pattern in order to produce the speckled scene

$$\Phi_X(u,v) = \Phi(u,v) \times X(u,v). \tag{3}$$

From each such random projection seen by the CCD camera, a scalar measurement y_m is obtained and stored in the computer. With incoherent light, this scalar measurement y_m corresponding to the summation of Eq. (2) can be performed with a lens focusing the incoherent wavefield onto a single pixel detector for summation of the intensities. In the coherent lighting conditions that we are investigating for compressive imaging, such an optical summation on the speckled field would produce interferences incompatible with Eq. (2). Instead,

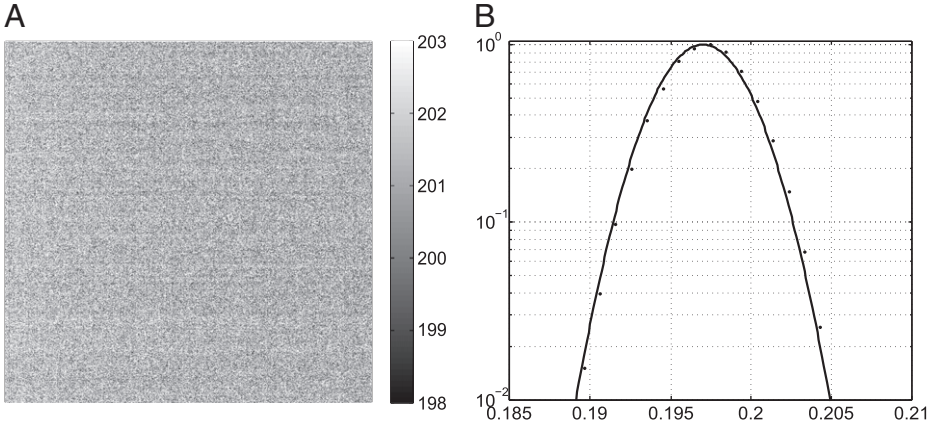

Fig. 2. (A) One realization of the thermal noise $B_1(u, v)$ at the CCD sensor of the camera; (B) Histogram of the intensities of panel (A). The camera used has a 10 bit dynamic with a 1024×1024 resolution. The 0–1023 digital dynamic is normalized to a [0,1] intensity scale.

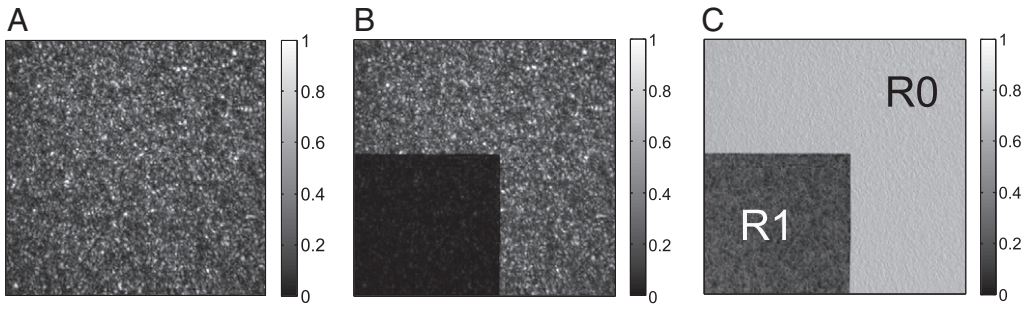

Fig. 3. (A) One realization of speckle $\Phi(u, v)$; (B) image of the speckled scene $\Phi_X(u, v)$ produced when the scene is placed in the speckle beam. (C) Ratio $R(u, v) = \frac{\Phi_X(u,v)}{\Phi(u,v)}$ between panel (B) and (A).

we propose to use a CCD as a means to perform a spatial conversion of local coherent field amplitudes into photo-electrons. Then, only the scalar value of the total number of photo-electrons created on the whole active surface of the CCD is required to obtain the scalar measurement y_m. We do that with a state-of-the-art CCD array, allowing also spatial XY information on the incident light field. But this XY information is not used, nor needed, for the compressive-imaging process. Only the total electric current (a single scalar) generated by the CCD array when illuminated is enough, in principle, for the compressive-imaging reconstruction. In practice, this could be obtained with a CCD device of much reduced complexity, specifically tailored for compressive sensing, having a "monolithic" structure with a single active element integrating the whole incident light field, and resembling more of a single planar photodiode, instead of a spatial XY array of a large number of active cells. But for convenience, to test the feasibility of the compressive sensing approach with coherent light, we use a much more common state-of-the-art CCD array, discard the spatial information, and use only a scalar sum from the array. The process of Eq. (3) is repeated for M distinct positions of the diffuser, to yield the M scalar measurements y_m of Eq. (2). The reproducibility of the positioning of the scene can be achieved in practice by working with speckle field with grain size much smaller than the typical dimension of the spatial contrasts in the scene. This can be controlled with the choice of the distance between the scene and the diffuser in Fig. 1. In case of a convergent beam, the closer the scene from the diffuser the smaller the grain size and reciprocally in case of a divergent beam. This is in perfect experimental conditions. In practice, some departure may exist from the perfect multiplicative action of the speckle described by Eq. (3). In this respect, the simple multiplication of two separate patterns in Eq. (3), and used as the basis of the compressive sensing scheme, would only be a useful approximation of the action of the speckle. In the sequel, we identify some relevant sources of departure existing in practice and observable with the experimental setup of Fig. 1. Then, we model and simulate their impact on the compressive sensing. And finally, we confront the picture with experiment in the setup of Fig. 1, for an assessment of the feasibility and robustness of the present optical implementation of compressive sensing.

4. Sources of noise

A first source of noise in the experimental setup of Fig. 1 is located at the sensor level due to thermal fluctuations in the CCD matrix. Fig. 2(A) presents one realization of this thermal noise acquired in darkness. As seen in Fig. 2(B), this thermal noise of the camera can be modeled as an additive Gaussian white noise $B_1(u, v)$ with standard deviation $\sigma_1 = 0.0026$. This constitutes a first perturbation to a pure recording of the multiplicative action of the speckle. The spatial average of noise $B_1(u, v)$ is found stationary for a given time exposure of the camera. This spatial average of noise $B_1(u, v)$ corresponds to the noise floor of the CCD camera which is systematically subtracted from the acquired image in the following.

A second perturbation directly impacts on the multiplication between the speckle beam $\Phi(u, v)$ and the scene to be imaged $X(u, v)$. Fig. 3(A) shows a speckle pattern $\Phi(u, v)$ produced after the diffuser of Fig. 1. When the scene $X(u, v)$ in Fig. 1, composed of a slide with calibrated levels carrying contrast, is placed in the speckle beam, the acquired image of Fig. 3(B) is observed for the speckled scene $\Phi_X(u, v)$. Fig. 3(C) presents the ratio $R(u, v) = \frac{\Phi_X(u, v)}{\Phi(u, v)}$ between the speckled scene $\Phi_X(u, v)$ and the speckle pattern $\Phi(u, v)$. In first approximation, the ratio image of $R(u, v)$ corresponds to the contrast carried by the slide introduced in the scene $X(u, v)$. Yet, as one inspects the histograms of the

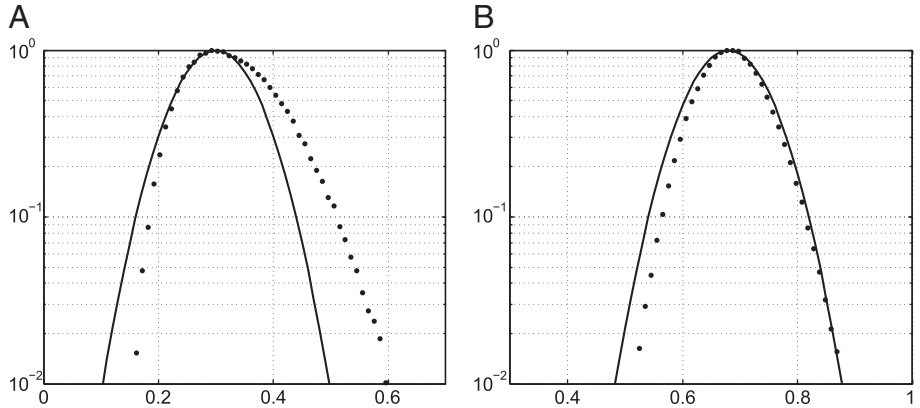

Fig. 4. (A) Histogram of the intensities of region R_1 of Fig. 3(C) in *log*. (B) Histogram of the intensities of region R_0 in Fig. 3(C) in *log*. Discrete dots (•) stand for the experimental counts. Solid lines stand for a Gaussian pdf with mean and standard deviation calculated from experimental counts in R_0 or in R_1. The standard deviation $\sigma_2 = 0.065$ is the same in both regions R_0 and R_1.

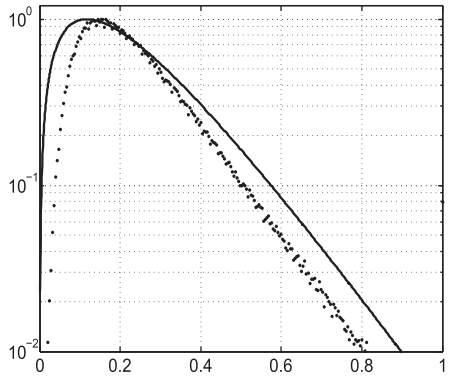

Fig. 5. Histogram of the intensities of Fig. 3(A). Solid line stand for a Gamma distribution with order $L=2$ and standard deviation $\sigma_S=0.23$ corresponding to a depolarized speckle pattern.

two regions composing $R(u, v)$, it appears that $R(u, v)$ is only matching $X(u, v)$ on average. This is visible in Fig. 4 where the pixels in $R(u, v)$ are distributed around the mean values expected in a pure multiplicative action of the speckle. This deviation from a pure multiplicative action of the speckle can be attributed to various causes such as spatial non uniformities of the calibrated slides in the scene $X(u, v)$, non-strictly planar incident wavefront of the laser beam, or residual mechanical vibrations in the experimental setup or also from natural convection in the air causing spatial fluctuations of the optical pathlength of the speckle scene $\Phi_X(u, v)$ randomly evolving in time. To better understand the impact of these perturbations on the experimental setup of Fig. 1, we propose to model this fluctuation with a multiplicative Gaussian white noise $B_2(u, v)$ with standard deviation $\sigma_2=0.065$ as observed from Fig. 4. As visible in Fig. 4, this model is not perfectly matching the experimentally observed histograms. We nevertheless consider this proposal as good enough for a second approximation model as a source, additional and independent from the sensor thermal noise, of departure from a pure recording of the multiplicative action of the speckle. The ratio of $\sigma_2/\sigma_1 \approx 25$ is considered sufficiently large to neglect the impact of the fluctuations of $B_1(u, v)$ in Fig. 3 once the noise floor has been removed. The typical structured patterns that are observed in $B_2(u, v)$ are not visible in $B_1(u, v)$, confirming a dominant character of the fluctuations in $B_2(u, v)$ over those in $B_1(u, v)$. From these observations, we consider that the influence of $B_1(u, v)$ on the estimation of $B_2(u, v)$ can reasonably be neglected. As a consequence, we propose to model the experimental action of the speckle in the following way

$$\Phi_{Xb}(u,v) = (\Phi(u,v) + B_2(u,v)) \times X(u,v) + B_1(u,v), \tag{4}$$

with $\Phi_{Xb}(u, v)$ as the experimental image acquired by the camera. We are now going to use this model to evaluate the robustness on the compressive sensing scheme to the experimental noises $B_1(u, v)$ and $B_2(u, v)$.

5. Simulation

We simulate the compressive imaging scheme in order to reconstruct the $N=8\times8$ binary image of Fig. 6(A) where the pixels of the image to be compressed are set to an intensity $I_1=0.75$ for the pixels of the object while the pixels of the background are set to $I_0=0.25$, in the absence of noise. To simulate the speckle patterns, we use the probability density $p_S(z)$, provided by the Gamma density

$$p_S^L(r) = \left(\frac{L}{\sigma_S}\right)^L \frac{r^{L-1}}{\Gamma(L)} \exp\left(\frac{-Lr}{\sigma_S}\right), \quad \text{for } r \geq 0, \tag{5}$$

where parameter L, called the speckle order, is an integer, σ_S is the standard deviation and the Gamma function can be written as $\Gamma(L) = (L-1)!$. As visible in Fig. 5, the speckle pattern produced by the experimental setup of Fig. 1 is in fair agreement with the Gamma density model of Eq. (5). In the following we will model the speckle pattern with a Gamma density of parameter $L=2$ corresponding to the experimental conditions observed in Eq. (5) for a fully depolarized speckle. Fig. 6(B) presents one realization of an $N=8\times8$ pattern of speckle with $\sigma_S=0.23$. Fig. 6(C) shows the reconstructed image $\hat{\mathbf{x}}$ obtained with $M=53$ scalar measurements y_m. The quality of the reconstructed image $\hat{\mathbf{x}}$ for a given number M of measurements can be assessed by the normalized cross-covariance $C_{\mathbf{x},\hat{\mathbf{x}}}$ given by

$$C_{\mathbf{x},\hat{\mathbf{x}}} = \frac{\langle(\mathbf{x}-\langle\mathbf{x}\rangle)(\hat{\mathbf{x}}-\langle\hat{\mathbf{x}}\rangle)\rangle}{\sqrt{\langle(\mathbf{x}-\langle\mathbf{x}\rangle)^2\rangle\langle(\hat{\mathbf{x}}-\langle\hat{\mathbf{x}}\rangle)^2\rangle}}, \tag{6}$$

where $\langle\cdot\cdot\rangle$ denotes the spatial average. Fig. 7 shows the global improvement of the normalized cross-covariance $C_{\mathbf{x},\hat{\mathbf{x}}}$ as a function of the number M of measurements for the binary image of Fig. 6(A). Additionally in Fig. 7, we compare, in terms of fraction of well-classified pixels, the input binary image $\mathbf{x}$ with a binarized version of the reconstructed image $\hat{\mathbf{x}}$. Perfect recovery is obtained in Fig. 7 with $M=53$ scalar measurements y_m after binarization by thresholding of $\hat{\mathbf{x}}$ at $(I_0+I_1)/2$ for the binary reference image of Fig. 6(A). This possibility of perfect recovery was found reproducible over multiple noise realizations with a high probability. We consider this result as a situation of reference for the compressive imaging scheme in absence of noise. We now study the evolution of the performance of the compressive imaging scheme for the reconstruction of the same image when the level of the two noises B_1 and B_2 in Eq. (4) is introduced. Fig. 8 presents the impact of the level of the additive Gaussian noise $B_1(u, v)$ or the multiplicative Gaussian noise $B_2(u, v)$ of Eq. (4) on the reconstruction of the image of Fig. 6(A) for the fixed number $M=53$ of scalar measurements y_m. Results from Fig. 8 are interesting since they allow to predict the performance of the compressive imaging scheme in various experimental

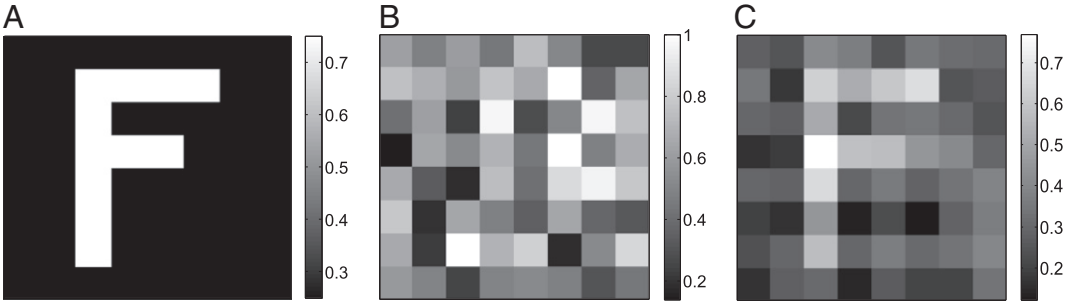

Fig. 6. (A) binary image with $N=8\times8$ pixels and intensity levels $I_1=0.75$ for the object and $I_0=0.25$ for the background; (B) one realization of speckle pattern with $\sigma_S=0.23$; (C) reconstructed image $\hat{\mathbf{x}}$ with $M=53$ scalar measurements y_m.

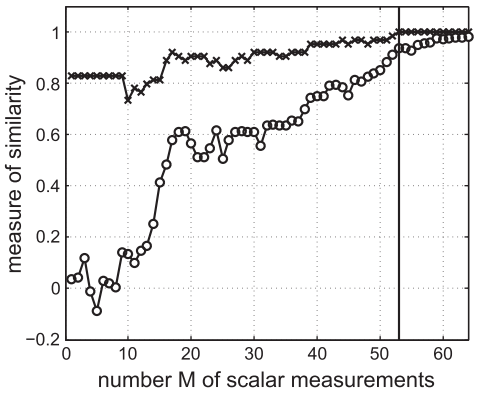

Fig. 7. Normalized cross-correlation (o) of Eq. (6) between the reference image of Fig. 6(A) and the reconstructed image $\hat{\mathbf{x}}$ and fraction of well-classified pixels (×) on the thresholded image of $\hat{\mathbf{x}}$ as a function of the number M of scalar measurements y_m.

conditions. For illustration, we have located the experimental levels of noise measured in our experimental setup. As visible in Fig. 8 our model predicts that, in such experimental conditions, the compressive imaging scheme should still succeed in the reconstruction of the observed image for $M=53$ scalar measurements y_m.

6. Experimental results

We are now ready to test the compressive sensing based on the experimental setup of Fig. 1. We propose to test it with a simple 8×8 binary input scene visible in Fig. 9(A) to confront our predictive model to experimentation. Fig. 10 presents the performance of reconstruction for this input image and it appears that a perfect reconstruction is possible from $y_m=20$ measurement therefore performing a 64:20 lossless compression ratio. For comparison, Fig. 10 also provides the simulation of the compressive sensing on the input image of Fig. 9(A) in the absence of noise and with the noise models tuned according to the experimental conditions. As visible in Fig. 10 the performance of the simulation reaches a perfect reconstruction almost for the same number of measurement $y_m=20$. This validates the capability of the noise model proposed in Eq. (4) to predict performance of the experimental optical implementation of the compressive sensing given in Fig. 1.

7. Discussion and conclusion

We have devised and tested an optical setup for an experimental implementation of compressive-sensing imaging. The key proposal is to exploit the speckle images arising with coherent light in order to realize the essential step of the multiplication with random references. An experimental setup for compressive imaging based on this proposal has been assembled and tested in its principle with simple 8×8 binary images. The results demonstrate the feasibility of the principle for compressive sensing, by achieving perfect experimental recovery of a compressed image of a typical 64:20 ratio. Compressive sensing has previously been implemented experimentally with Gaussian distributions or Bernoulli binary distributions. The speckle intensity is following exponential distributions. Our result therefore extends the scope of distributions that can be found in practice and that can be used for practical implementation of compressive sensing. Concerning the compression performances, the compression rate achieved depends on various parameters since it is not only image dependent but also relies on the projection basis used for the compressive sensing. Therefore, the compression performance is essentially given here as a typical value and as an additional proof of feasibility. As another original contribution of the present report, we have identified some relevant sources of noise and simulate their impact on the compressive sensing. This quantitatively establishes the robustness of the optical compressive-sensing imaging scheme introduced in this report.

In the previously proposed experimental setups for compressive imaging, the random projections of Eq. (2) are usually realized through the intervention of mechanical material elements. For instance, in the incoherent optical imaging system of [4,5], an array of micro-mirrors is electrically flipped to create pseudo-random patterns that are successively applied to affect the transmission of an input image. In the terahertz imaging system of [23,24], the random projections are realized by copper plates irregularly pierced by holes and mechanically translated to intercept a terahertz beam also traversing a planar mask (the imaged object) between two antennas. As an alternative here, we have shown that a coherent light could naturally offer a simple way to perform such a multiplication with a random pattern, under the form of a speckle image. The ability of this mode of operation to realize the random projections of compressive sensing is validated here by the possibility of perfect reconstruction that was obtained. This proof of feasibility concerning an all-optical implementation of the essential step of the random projections was obtained here in a simple configuration of the optical setup of Fig. 1. The aim was to concentrate on proving the feasibility of the principle, by means of a setup configuration with low complexity. In particular, the small 8×8 size of the image brought the facility of a small number of diffuser positions to manage, resulting in a small number of random references. However, the scheme in principle can be extended to larger images, with a larger number of random references to handle. In such conditions of operation, the random speckle patterns of reference produced by the diffuser at different

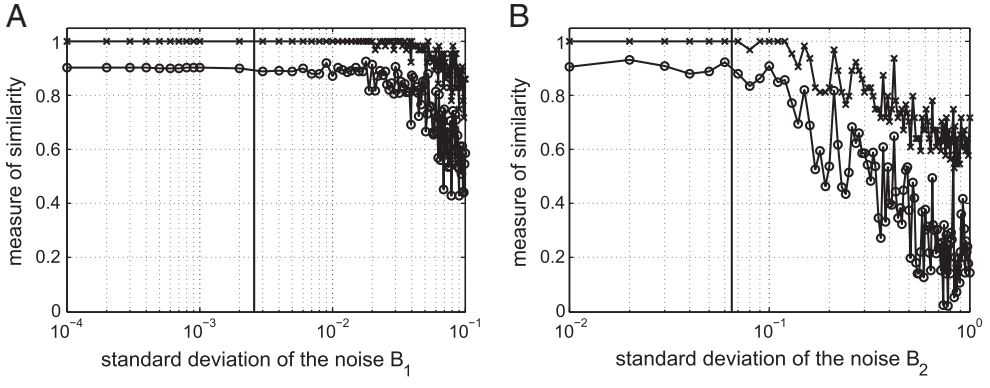

Fig. 8. (A) Normalized cross-correlation (o) of Eq. (6) between the reference image Fig. 6(A) and the reconstructed image $\hat{\mathbf{x}}$ Fig. 6(C) and fraction of well-classified pixels (×) on the thresholded image of $\hat{\mathbf{x}}$ as a function of the standard deviation σ_1 of the noise $B_1(u,v)$ for a fixed number $M=53$ of scalar measurement y_m. The level of noise $B_2(u,v)$ is zero. Panel (B) same as panel (A) but noise level of noise $B_1(u,v)$ is zero and the level σ_2 of noise $B_2(u,v)$ is raised. In (A) and (B) the solid vertical lines stand for the levels of noise present in our experimental setup.

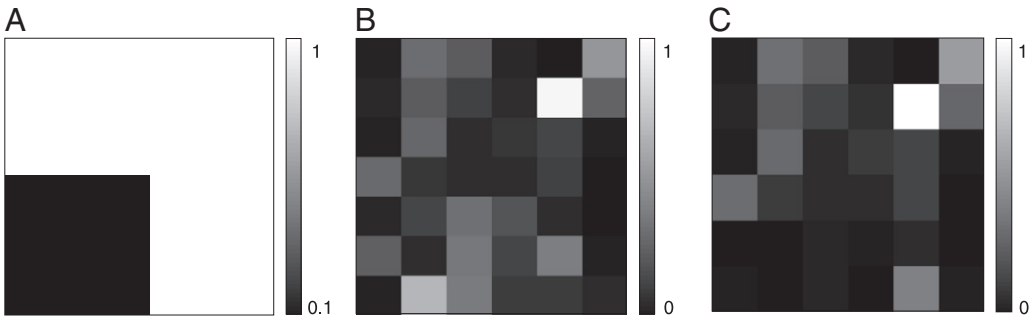

Fig. 9. (A) Optical version of the input image to be compressed with $N=8\times8$ pixels and intensity levels $I_0=1$ and $I_1=0.1$. (B) One experimental realization of a speckle pattern with $N=8\times8$ pixels. (C) Multiplication of this speckle pattern by the input image $X(u, v)$ optically realized with the setup of Fig. 1.

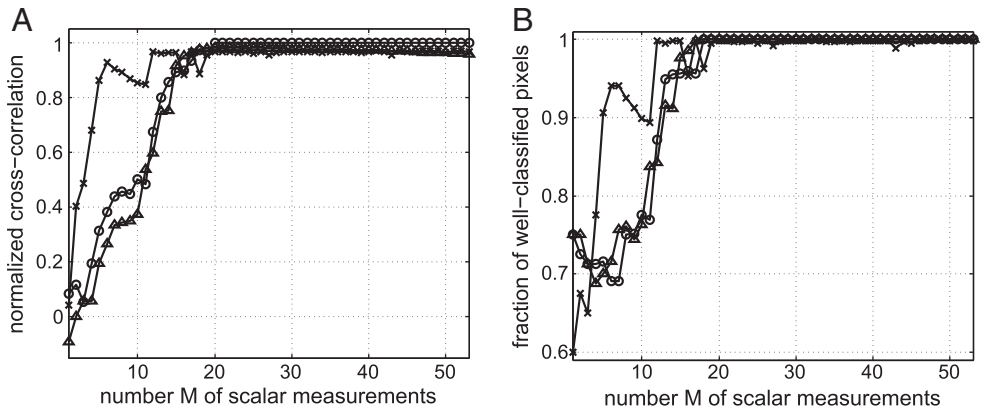

Fig. 10. (A) Normalized cross-correlation of Eq. (6) between the reference image Fig. 9(A) and the reconstructed image $\hat{\mathbf{x}}$ as a function of the number M of scalar measurements y_m: (o) averaging over 10 realizations for the simulated reference situation with no noise, (△) averaging over 10 realizations for simulated reconstruction of Fig. 9(A) in our experimental conditions of noise with $\sigma_1=0.0026$ and $\sigma_2=0.065$, (×) averaging over 10 realizations for the reconstruction of Fig. 9(A) for images acquired via the experimental setup of Fig. 1. (B) same as (A) but with fraction of well-classified pixels between the reference binary image Fig. 9(A) and the thresholded image of $\hat{\mathbf{x}}$.

spatial positions, could be measured once and for all and attached to a given optical compressive-sensing setup, by assuring reproducible spatial positioning of the diffuser at sufficient precision. Alternative ways could be examined to control the realization of reproducible random-like speckle patterns, for instance with electro-optical devices (spatial light modulators, digital micro-mirror devices). The typical size of the pixels of such devices is much larger than the wavelength. In such condition, it has recently been shown [25] theoretically and experimentally that a quasi optical geometric regime is accessible that allows to use an optical summation with a lens and a single-pixel detector like in coherent compressive imaging. In our case, a simple frosted glass was used instead. The perturbation of the wavefield by the diffuser is made at the wavelength scale. The intensities of the resulting speckled images cannot be summed optically as explained in Section 3. Electro-optical devices could also be used to generate the image to be compressed with more sophisticated structured images with higher resolution and also with multiple gray levels instead of binary images. Another useful evolution would be to test the imaging process on an arbitrary three-dimensional scene. In its present form, the optical setup of Fig. 1 obtained compressive acquisition of an image materialized by a slide with spatially distributed transparency. It was also the same type of slide object that was used in previously proposed experimental setups for compressive imaging [4,5,23,24], as convenient laboratory condition for the test of an innovative implementation principle. A further step with our setup would be to test its principle with a three-dimensional scene illuminated by the speckled coherent beam. It should then be verified that the result can still be analyzed as an image of the underlying scene multiplied by a known random speckle pattern. If the three-dimensional scene displays significant microscale irregularities, it can even generate its own speckle pattern that would also act multiplicatively in the measured image. In this case, the compressive-sensing scheme, if it still operates, would reconstruct an image of the scene carrying its own speckle. The reconstructed image would in fact have the appearance of a coherent image as measured with common coherent imaging devices, however acquired via compressive sensing. Such evolutions represent further steps to investigate, beyond the demonstration given here of the potential of multiplicative speckle patterns for compressive sensing, and in order to progress toward more practical and flexible compressive-imaging devices. Since coherent imaging exists outside optics, for instance with acoustic sonar or radiowave SAR imagings, the present results could also hold potentialities for compressive sensing in these areas.

References

[1] E. Candès, J. Romberg, T. Tao, IEEE Transactions on Information Theory 52 (2) (2006) 489.
[2] D. Donoho, IEEE Transactions on Information Theory 52 (4) (2006) 1289.
[3] J. Haupt, R. Nowak, IEEE Transactions on Information Theory 52 (9) (2006) 4036.
[4] J. Romberg, IEEE Signal Processing Magazine 25 (2) (2008) 1053.
[5] M. Duarte, M. Davenport, D. Takhar, J. Laska, T. Sun, K. Kelly, R. Baraniuk, IEEE Signal Processing Magazine 25 (2) (2008) 83.
[6] R. Robucci, J. Gray, L. Chiu, J. Romberg, P. Hasler, Proceedings of the IEEE 98 (6) (2010) 1089.
[7] L. Jacques, P. Vandergheynst, A. Bibet, V. Majidzadeh, A. Schmid, Y. Leblebici, IEEE International Conference on Acoustics, Speech and Signal Processing (ICASSP), 2009, p. 1113.
[8] R. Marcia, Z. Harmany, R. Willett, Proc. IS&T/SPIE Symposium on Electronic Imaging: Computational Imaging VII, 2009.
[9] M. Neifeld, J. Ke, Applied Optics 46 (22) (2007) 5293.
[10] P. Baheti, M. Neifeld, Optics Express 16 (3) (2008) 1764.

[11] A. Stern, B. Javidi, Journal of Display Technology 3 (3) (2007) 315.
[12] Y. Rivenson, A. Stern, B. Javidi, Optics Express 18 (14) (2010) 15094.
[13] J. Goodman, Speckle Phenomena in Optics: Theory and Applications, Roberts & Company, Greenwood Village CO, 2008.
[14] P. Réfrégier, Noise Theory and Application to Physics: From Fluctuations to Information, Springer Verlag, New York, 2006.
[15] O. Katz, Y. Bromberg, Y. Silberberg, Applied Physics Letters 95 (13) (2009) 131110.
[16] A. Gatti, M. Bache, D. Magatti, E. Brambilla, F. Ferri, L. Lugiato, Journal of Modern Optics 53 (5) (2006) 739.
[17] L. Basano, P. Ottonello, Optics Communications 282 (14) (2009) 2741.
[18] S. Blanchard, D. Rousseau, D. Gindre, F. Chapeau-Blondeau, Optics Letters 32 (14) (2007) 1983.
[19] S. Blanchard, D. Rousseau, D. Gindre, F. Chapeau-Blondeau, Optics Communications 281 (17) (2008) 4173.
[20] Y. Rivenson, A. Stern, IEEE Signal Processing Letters 16 (6) (2009) 449.
[21] M. Harwit, N. Sloane, Hadamard transform optics, Academic, New York, 1979.
[22] S. Kim, K. Koh, M. Lustig, S. Boyd, D. Gorinevsky, Journal on Selected Topics in Signal Processing 1 (2007) 606.
[23] W. Chan, K. Charan, D. Takhar, K. Kelly, R. Baraniuk, D. Mittleman, Applied Physics Letters 93 (12) (2009) 121105.
[24] W. Chan, M. Moravec, R. Baraniuk, D. Mittleman, Conference on Lasers and Electro-Optics (CLEO), 2007, p. 1.
[25] M. Zambrano-Nũnez, E. Marango, J. Fisher, IEEE Workshop on Signal Processing Systems (2010) 111.